IEEE **Photonics** Journal
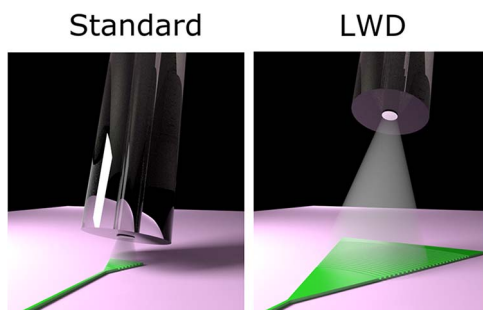
An IEEE Photonics Society Publication

Open Access

Long-Working-Distance Grating Coupler for Integrated Optical Devices

Volume 8, Number 1, February 2016

C. J. Oton

Standard   LWD

Long-Working-Distance Grating Coupler for Integrated Optical Devices

C. J. Oton

Istituto di Tecnologie della Comunicazione dell'Informazione e della Percezione (TeCIP),
Scuola Superiore Sant'Anna, 56124 Pisa, Italy

Abstract: A novel grating coupler design is presented with its experimental demonstration. The grating can focus the outcoming light upward without the need for a lens or additional fabrication steps. The lenslike effect is introduced by applying a deformation to the grating stripes in order to add a phase map that matches the phase of the spherical wavefront coming from the fiber. The presented grating is designed for silicon photonics technology and has a working distance of 230 μm to a standard single-mode fiber. This long distance would introduce an excess loss of 9 dB with a standard grating, whereas with the long-working-distance grating, we demonstrate no extra loss with respect to the standard grating.

Index Terms: Integrated optics, gratings, silicon photonics.

1. Introduction

Optical coupling from standard single-mode fibers (SMF) to semiconductor waveguides is a challenging issue due to the beam size mismatch, which is about 10 μm for the fiber and about 500 $\times$ 220 nm for a typical single-mode silicon waveguide. Both vertical [1] and butt-coupling [2] solutions are possible; however, if very broad coupling bands are not required, vertical coupling schemes based on grating couplers are usually preferred. The main advantage of grating couplers are the possibility of coupling light without the need of an edge, which makes edge preparation unnecessary, and allows for wafer-scale testing before dicing. Grating couplers have been very extensively investigated during the last decade, and very efficient coupling ratios have been demonstrated, especially when additional fabrication steps are included in the process, like thickening the silicon-on-insulator (SOI) layer [3] or introducing a high reflector in the substrate [4]. All these gratings adapt the output of the light to match the size of the mode of a single-mode fiber. A typical solution includes the focusing to the waveguide through an elliptical curvature of the grating stripes, which reduces the footprint of the grating. However, these solutions only provide low loss when the fiber cross-section is set very close to the surface of the optical circuit. However, there are many situations in which this may not be possible. Fig. 1 shows some examples of these situations, for instance, if there are obstacles that prevent a close approach of the tip of the fiber to the surface or if the fiber is set horizontally and the light must be bent downwards with a flat mirror. In these cases, the output beam from the fiber starts to expand, with its wavefront becoming spherical after a few tens of microns; therefore, a beam focusing lens or curved mirror have been the only possible ways of keeping good coupling efficiency so far [5], [6].
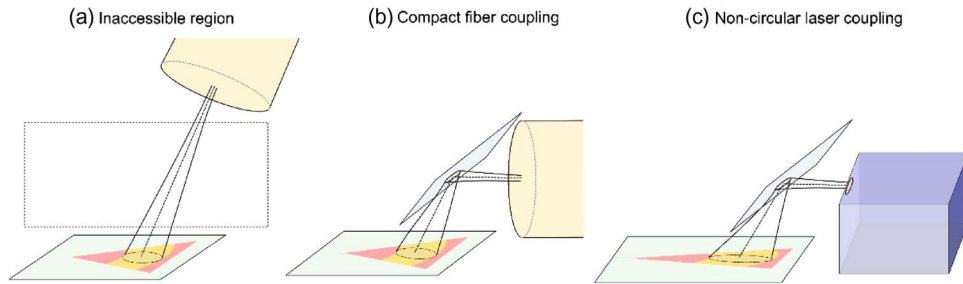
Fig. 1. Application examples of the long-working-distance (LWD) grating coupler technology. (a) Inaccessible region prevents a close approach of the fiber. (b) Horizontal fiber output is bent by a flat mirror, without loss due to extra distance. (c) Gratings can be tailored to adapt to any beam shape, for example, elliptical beams.
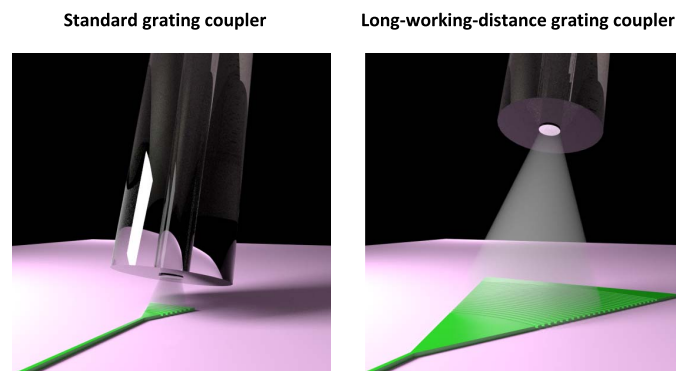

Fig. 2. (Left) Working principle of a standard grating coupler and (right) long-working-distance grating coupler. The LWD grating is larger than the standard one but allows for coupling from much longer distances.

In this paper, we propose an alternative way of focusing the expanded beam of the fiber by emulating the action of a lens through the introduction of a phase map which matches the one of a typical lens. With this grating, we experimentally demonstrate a working distance of 230 μm and the same coupling efficiency with respect to a standard grating coupler at its optimum working distance.

2. Working Principle

The principle of the proposed grating is shown in Fig. 2. When a Gaussian beam propagates in free space along the z axis, its beam radius w has the following dependence on z [7]:

$$w(z) = w_0 \sqrt{1 + \left(\frac{z}{z_R}\right)^2} \tag{1}$$

where w_0 is the beam radius at which the field amplitude decays to $1/e$, and z_R is the so-called *Rayleigh range*, which is equal to

$$z_R = \frac{\pi w_0^2}{\lambda_0} \tag{2}$$

where λ_0 is the vacuum wavelength of the light. The Rayleigh range can be considered as a threshold distance between a flat and a spherical wavefront. This means that beyond the
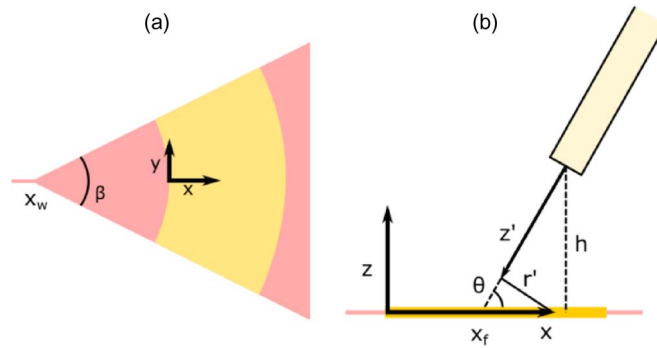
Fig. 3. Geometrical sketch and variable definitions. (a) Top view. (b) Side view.

Rayleigh range, the beam can no longer be considered collimated, and it starts to expand, becoming a spherical wavefront. The Rayleigh range of the output of a standard SMF is equal to 56 μm at 1.55 μm wavelength considering a beam diameter of 10.5 μm. This means that beyond a distance of 56 μm, the coupling efficiency of a grating coupler starts to decrease considerably.

Setting the fiber at 230 μm from the grating, the beam diameter becomes 44 μm-wide, which clearly yields a very low efficiency if we use a standard grating with a total size of about 12 μm. To recover a good coupling efficiency we need a larger grating size to match the beam, and we need to correct the spherical shape of the wavefront by deforming the stripes of the grating. At this point, we have two options: i) We can collimate the beam, which would generate a very wide collimated mode on a $\sim$50 $\times$ 0.22 μm waveguide, which would then require a very long adiabatic taper to narrow it down to 500 nm, or more conveniently, ii) we can refocus the beam in order to generate another spherical beam which directly focuses the light on a 500 nm waveguide, as it is usually done in order to make compact couplers. For that reason, we opt for (ii). Therefore, the stripes in our grating convert the spherically tilted wavefronts from the fiber to spherical waves which focus at the tip of the grating. In other words, what we are doing is emulating a single $\sim$50 μm-wide spherical lens which collects and refocuses the spherical beam from the fiber to the single-mode waveguide. The advantage of this approach with respect to setting a lens at the output of the fiber is clear, as a lens is an extra element which also requires alignment to the fiber and to the grating, while the long-working-distance (LWD) grating does not require extra elements or fabrication steps, and is automatically aligned to the waveguide.

3. Design and Simulations

Fig. 3 shows the variable definitions for a triangular LWD grating design for TE polarization. The procedure we used is the following. We first calculate with (1) how much the beam expands from the fiber tip to the surface of the grating, to give us a magnitude of the grating size, which in our case is 44 μm as previously mentioned. Then, we start with a design of a standard (constant) grating in 2D with Finite Difference Time Domain (FDTD) with the desired angle to a hypothetical fiber of 44 μm beam diameter. Such large beam diameter requires a very low duty cycle, as typical gratings made with shallow etch values of $\sim$70 nm have a scattering efficiency optimized for a $\sim$12 μm beam size, but a 44 μm beam requires much lower scattering strength, so we optimize the duty cycle to obtain a scattering efficiency which matches best with a Gaussian beam of 44 μm-diameter. This corresponds to about 15% duty cycle, meaning a 15% etched region in a single period. This also allows for the calculation of the effective index of the grating region n_{eff}.

Once the duty-cycle and the n_{eff} are calculated, we can calculate the shape of the stripes. We can do this by first calculating the phase ϕ_w of the circular wave that propagates and expands
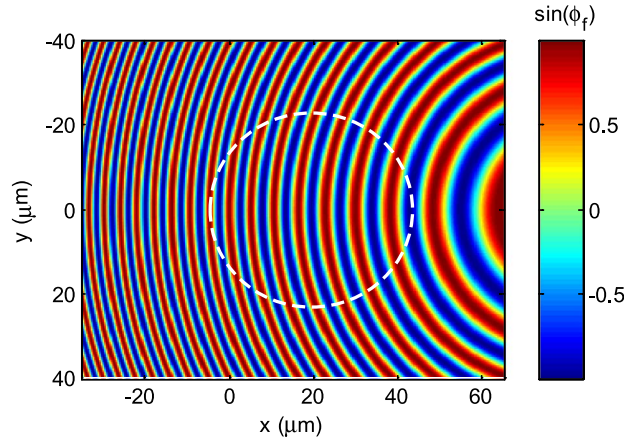
Fig. 4. Phase map of a beam of a 14° tilted SMF at a height of 230 μm from the surface. The white dashed ellipse marks the beam profile at 1/e electric field. The axis of the fiber intersects at the point (20, 0). The origin marks the position of the first line of the grating.

through the aperture of the triangular grating. In this case, we can approximate the wavefronts as pure circumferences as we are far away from the Rayleigh distance of the aperture:

$$\phi_w(x, y) = \frac{2\pi n_{eff}}{\lambda_0} \sqrt{(x - x_w)^2 + y^2} \tag{3}$$

where n_{eff} is the effective index of the grating mode, and x_w is the aperture origin as shown in Fig. 3(a). With this approximation, there is a phase offset in the phase values due to the non-Rayleigh region and also due to the fact that the effective index in the non-striped region is not n_{eff}, but this offset does not influence the result as we are only interested in the wavefront shape.

Then we calculate the 2D profile of the phase of the Gaussian beam coming out of the fiber which illuminates the surface of the grating. The fiber is tilted (14°) to reduce back-reflections, as is usually done in standard grating couplers, and we set its height to 230 μm. Using the primed variables defined in Fig. 3(b), we apply the general equation of Gaussian beams in free space [7]

$$\phi_f(z', r') = \frac{2\pi n_0}{\lambda_0} \left(z' + \frac{r'^2}{2R(z')} \right) - \zeta(z') \tag{4}$$

where ϕ_f is the phase of the Gaussian beam; n_0 the refractive index of the medium, which is air in our case; $R(z')$ the radius of curvature of the wavefront; and $\zeta(z')$ is the Gouy phase, which is defined as

$$R(z') = z \left[1 + \left(\frac{z_R}{z'} \right)^2 \right] \tag{5}$$

$$\zeta(z') = \arctan\left(\frac{z'}{z_R} \right). \tag{6}$$

Equation (4) has been applied to extract the phase map shown in Fig. 4, where the variables have been remapped to (x, y) along the surface of the grating. Finally, in order to extract the position of the grating stripes, we only have to sum both phases $\phi_w(x, y) + \phi_f(x, y)$ and mark the 2π integer multiples. These lines mark the central points of the stripes.

The position of the stripes establish the grating period, which varies along the grating to introduce the upward-focusing feature. The variation is not linear, (although a linear approximation may be possible depending on the angle), because the wavefront is curved. The period starts at
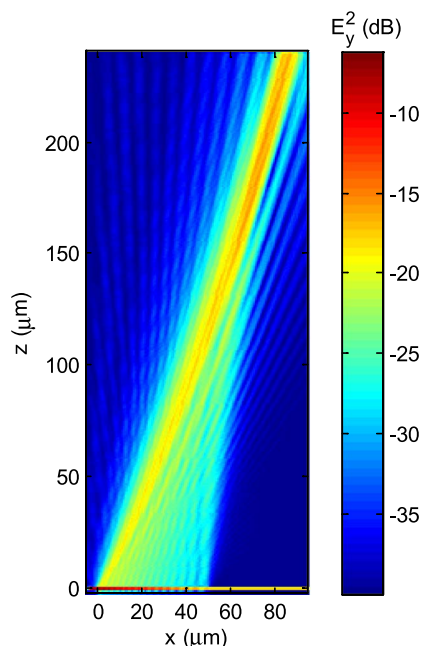
Fig. 5. FDTD simulation where the upward focusing effect is observed. The grating first stripe is at the origin.

568 nm and finishes at 622 nm. On the other hand, the width of the stripes is calculated from the duty cycle, which we previously fixed to 15%. To improve efficiency, one could gradually vary the duty cycle too to obtain a better match with a Gaussian shape. However, in our case we just considered a constant duty cycle for simplicity. As the period of the grating is not constant, neither is the stripe width, which consequently varies between 85 and 93 nm. These narrow trench widths are possible using e-beam lithography, which is the fabrication process we used in this work. Being aware that these widths are too narrow for deep-UV lithography, possible solutions can be proposed to keep wider trench depths. The simplest one would be to reduce the shallow-etch depth, which would allow us to set duty cycles around 50%, although would alter the fabrication process flow. Alternatively, one could limit the scattering efficiency by introducing subwavelength features or circular holes [8], [9].

A final simulation of the grating was done by 2-D FDTD in order to establish the optimum fiber lateral displacement with respect to the first grating line [x_f as shown in Fig. 3(b)], which was 20 μm for our case. The focusing effect is clearly observed in the simulation shown in Fig. 5. The designed grating has an expected efficiency of –2.5 dB at 1550 nm in a 2-D approximation, in which the reflection from the bottom of the buried oxide was considered. Finally the designed and fabricated grating coupler with an aperture angle $\beta = 40°$ is shown in Fig. 6.

4. Fabrication and Characterization

The sample was fabricated in the Valencia Nanophotonics Technology Center, Spain. The initial wafer was a silicon-on-insulator (SOI) wafer with 220 nm silicon thickness and 2 μm buried oxide. Electron-beam lithography was used for defining the etched areas. First, a shallow-etch of 70 nm was defined along the stripes of the grating, followed by a full-etch step to engrave the triangle and the connecting waveguides. Identical input and output gratings were drawn with a lateral shift to avoid non-coupled reflected light from reentering the fiber. In the same run, standard flat gratings were also included for reference. These have a width of 12 μm, a duty cycle of 50% and a constant period of 630 nm, which are optimized values for 70 nm etch depth and TE polarization.
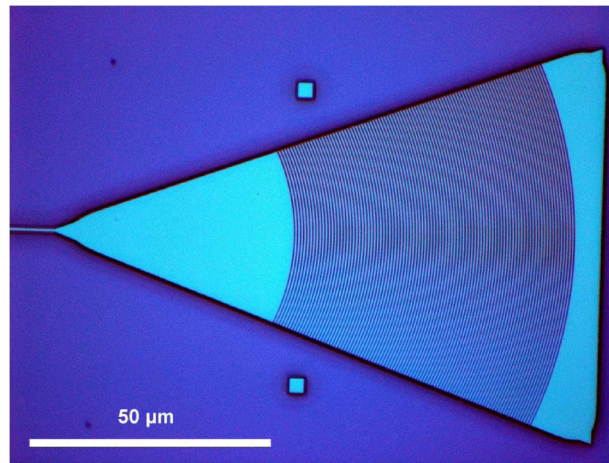
Fig. 6. Optical micrograph of the fabricated LWD grating coupler. The stripes are not pure ellipses, as in an standard grating, but are deformed according to the phase map shown in Fig. 4. Inaccuracies at the angles of the triangle are due to corner effects in e-beam lithography.
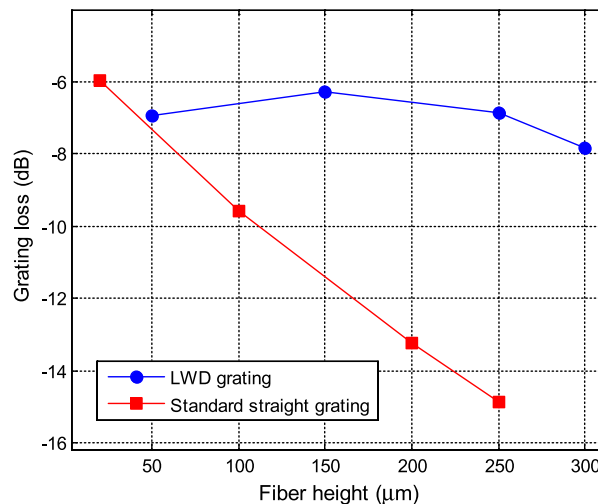

Fig. 7. Experimental grating loss at 1550 nm versus fiber height for the LWD grating and a standard straight grating. The long-working-distance behavior of the former is clearly observed.

The gratings were characterized by aligning optical input and output single-mode fibers to the structures. A tunable laser was used as a source, setting an input power of 1 mW. The polarization was first optimized using a polarization controller, and then, the fibers were aligned by optimizing the signal at different fiber heights, which were measured using the fiber holder micropositioners. The grating loss was calculated by dividing the total loss by a factor of 2 in dB units, as reciprocity imposes input and output efficiencies to be the same.

Grating loss at 1550 nm versus fiber height is reported in Fig. 7 for both standard and LWD gratings. While the peak loss values of both is almost the same (~6 dB), the dependence of the loss with fiber distance is very different. While the LWD keeps a good coupling efficiency along hundreds of microns of distance, the standard grating efficiency rapidly decays. The coupling efficiency in both gratings is lower than the simulated efficiency (where 3 dB loss was expected), most likely due to fabrication deviations (in terms of etch depth, trench width or other fabrication inaccuracies), because it affects both the LWD grating and the standard grating. Regarding the alignment, we did not find the LWD grating to be more or less sensitive to
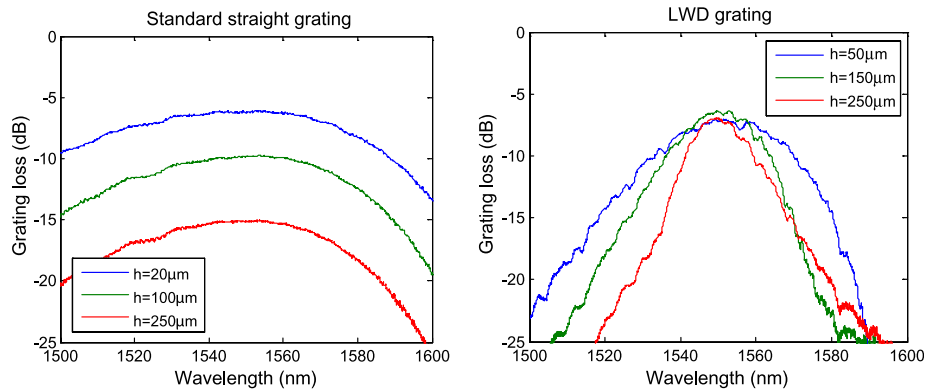
Fig. 8. Grating loss spectra of a (left) standard straight grating and (right) LWD grating.

position alignment versus the standard grating. This is expected, as the image size of the focused beam is designed to match the one of the SMF fiber.

Spectra of the grating loss is shown in Fig. 8. It is worth noting that the bandwidth of the LWD is narrower than standard grating. While the standard grating has a constant 3 dB bandwidth of 82 nm, regardless of the distance, the 3 dB bandwidth of the LWD grating decreases from 37 nm (at 50 μm height) to 18 nm (at 250 μm height). This is an expected behavior of a longer grating, because the more grating stripes contribute to the image formation, the more sensitive to wavelength the grating tends to be. This is an intrinsic limitation of larger gratings, although it can be partially alleviated by dispersion engineering the grating region to make it less wavelength dependent [10]. In any case, this limitation should not be a problem in certain applications, for example when the light source to be coupled to the waveguide has a limited bandwidth.

We already mentioned two applications in which LWD gratings may be useful [see Fig. 1(a) and (b)]. But nothing prevents us to adapt not only a spherical wavefront, but any known wavefront approaching the grating. For instance, typical laser output beams have an elliptic shape [Fig. 1(c)]. In these cases, it is not difficult to modify the stripe-shape calculation by introducing elliptic beams, which would require substituting (4) with the appropriate analytical shape from an elliptic Gaussian beam. This would avoid the need for optical elements such as prisms or aspherical lenses for wavefront correction. Finally, the example presented in this paper is applied to silicon photonic technology; however this concept can be applied to any integrated optical technology.

5. Conclusion

We propose a novel concept in grating coupler design which we call long-working-distance grating. The tailoring of the phase map of the grating allows for much further working distances without a penalty in coupling loss due to beam expansion. We experimentally demonstrated its functionality with the design and fabrication of a grating coupler capable of working at a height of 230 μm with the same coupling loss of a standard grating coupler and not requiring a lens or curved mirror.

Acknowledgment

References

[1] G. Roelkens *et al.*, "Bridging the gap between nanophotonic waveguide circuits and single mode optical fibers using diffractive grating structures," *J. Nanosci. Nanotechnol.*, vol. 10, no. 3, pp. 1551–1562, Mar. 2010.
[2] B. Ben Bakir *et al.*, "Low-loss (< 1 dB) and polarization-insensitive edge fiber couplers fabricated on 200-mm silicon-on-insulator wafers," *IEEE Photon. Technol. Lett.*, vol. 22, no. 11, pp. 739–741, Jun. 2010.

[3] D. Vermeulen *et al.*, "High-efficiency fiber-to-chip grating couplers realized using an advanced CMOS-compatible silicon-on-insulator platform," *Opt. Exp.*, vol. 18, no. 17, pp. 18 278–18 283, Aug. 2010.

[4] W. S. Zaoui *et al.*, "Cost-effective CMOS-compatible grating couplers with backside metal mirror and 69% coupling efficiency," *Opt. Exp.*, vol. 20, no. 26, pp. B238–B243, Dec. 2012.

[5] Y. M. Sabry, B. Saadany, D. Khalil, and T. Bourouina, "Silicon micromirrors with three-dimensional curvature enabling lensless efficient coupling of free-space light," *Light Sci. Appl.*, vol. 2, no. 8, p. e94, Aug. 2013.

[6] T. Tekin, "Review of packaging of optoelectronic, photonic, and MEMS components," *IEEE J. Sel. Topics Quantum Electron.*, vol. 17, no. 3, pp. 704–719, May/Jun. 2011.

[7] O. Svelto, *Principles of Lasers*, 5th ed. Berlin, Germany: Springer-Verlag, 2010.

[8] R. Halir *et al.*, "Continuously apodized fiber-to-chip surface grating coupler with refractive index engineered subwavelength structure," *Opt. Lett.*, vol. 35, no. 19, pp. 3243–3245, Oct. 2010.

[9] L. Liu, M. Pu, K. Yvind, and J. M. Hvam, "High-efficiency, large-bandwidth silicon-on-insulator grating coupler based on a fully-etched photonic crystal structure," *Appl. Phys. Lett.*, vol. 96, no. 5, Feb. 2010, Art. ID 051126.

[10] R. Halir *et al.*, "Colorless directional coupler with dispersion engineered sub-wavelength structure," *Opt. Exp.*, vol. 20, no. 12, pp. 13 470–13 477, Jun. 2012.